Fermi surface topology and de Haas–van Alphen orbits in $PuIn_3$ and $PuSn_3$ compounds

C.-C. Joseph Wang,[1] M. D. Jones,[2] and Jian-Xin Zhu[1]

[1]*Theoretical Division, Los Alamos National Laboratory, Los Alamos, New Mexico 87545, USA*

[2]*Department of Physics and Center for Computational Research, University at Buffalo–SUNY, Buffalo, New York 14260, USA*

(Received 5 April 2013; revised manuscript received 16 July 2013; published 5 September 2013)

Since the recent discovery of plutonium-based superconductors such as $PuCoIn_5$, systematic studies of the electronic properties for plutonium compounds are providing insight into the itinerancy-localization crossover of Pu $5f$ electrons. We are particularly interested in understanding the Fermi surface properties of the $PuIn_3$ compound, which serves as the building block for the $PuCoIn_5$ superconductor. Motivated by the first observation of quantum oscillation and renewed interest in the de Haas–van Alphen (dHvA) measurements on $PuIn_3$, we study the Fermi surface (FS) topology and the band dispersion in both the paramagnetic and antiferromagnetic states of $PuIn_3$, based on density-functional theory with a generalized gradient approximation. We compare the results with its isostructural paramagnetic compound $PuSn_3$. We present the detailed Fermi surfaces of the compounds $PuIn_3$ and $PuSn_3$, and conclude that the FS topology of an antiferromagnetic $PuIn_3$ agrees better with dHvA measurements. In addition, we show the magnetization of the antiferromagnetic order can alter the field-angle dependence and values of the effective mass for the dHvA orbits. Our results suggest that the accurate determination of the magnetic order orientation with respect to the crystal orientation is crucial to advance the understanding of the electronic structure of the $PuIn_3$ compound.

DOI: 10.1103/PhysRevB.88.125106 PACS number(s): 71.18.+y, 71.20.−b, 71.27.+a, 74.70.Tx

I. INTRODUCTION

Actinide metals[1] are strongly correlated electronic systems due to the narrow bandwidth of $5f$ electrons. In addition, a strong spin-orbit interaction within the $5f$ electron systems comparable to other energy scales renders the understanding of the electronic properties of the actinide metals more difficult. The itinerant-to-localized crossover of $5f$ electrons that occurs near plutonium in the actinide series is one of the most challenging issues in condensed matter physics, partly because the dual character (partially localized and delocalized) of these $5f$ electrons is closely related to the abrupt atomic volume variation between the α-Pu and δ-Pu metals. This change in bonding leads to a 25% larger volume in the δ phase as opposed to a low-symmetry, monoclinic crystal structure α phase of Pu, along with a variety of unusual physical and mechanical properties.[2–4]

To understand the $5f$ electron delocalization-localization crossover in elemental actinide solids, it is very helpful to gain insight by studying its derivative compounds, which also show other emergent properties. One of the noticeable Pu-based compounds are 115 series. It has been discovered recently that superconductivity occurs in $PuCoGa_5$ (Ref. 5) ($T_c = 18.5$ K), $PuRhGa_5$ (Ref. 6) ($T_c = 8.7$ K), and $PuCoIn_5$ (Ref. 7) ($T_c = 2.5$ K) series. The detailed pairing mechanisms in Pu-115 compounds are currently under intense investigation.[8,9] We are particularly interested in the electronic properties of $PuIn_3$ and its isostructural partner $PuSn_3$. The reasons are twofold. First, the $PuCoIn_5$ structure consists of stacked $CoIn_2$ and $PuIn_3$ layers, therefore the understanding of the electronic properties in $PuIn_3$ is relevant to uncovering the mystery of superconductivity in $PuCoIn_5$. Second, the recent experimental capability to measure the Fermi surface topology of $PuIn_3$ by de Haas–van Alphen (dHvA) effects can help narrow down the minimal effective theory for these complicated systems.

In this paper, we present systematic studies on the electronic structures of $PuIn_3$ and $PuSn_3$ within density-functional theory (DFT). We calculate the band dispersion, density of states (DOS), and the Fermi surface topology, together with the identification of extremal dHvA orbits. For $PuIn_3$, there is recent experimental evidence[10] that the ground state of $PuIn_3$ is antiferromagnetic (AFM). However, the earlier dHvA measurement in this compound has been improperly interpreted in terms of DFT calculations based on a paramagnetic (PM) state of $PuIn_3$.[11] In the present work, we show the Fermi surface extremal orbits obtained for AFM $PuIn_3$ are in good agreement with the dHvA measurements, which makes the theory and experiment comparison more consistent. Also, with the known experimental fact that $PuSn_3$ is paramagnetic in the ground state, we predict a quite different band structure and Fermi surface topology in $PuSn_3$ as opposed to PM $PuIn_3$. An experimental verification of this prediction provides strong support for Landau's Fermi liquid theory and demonstrates the potential toward the detection of quantum oscillations in the δ phase of Pu.

The organization of this paper is as follows. In Sec. II, we describe our theoretical method and briefly review the dHvA effects in itinerant electronic systems such as metals. In Sec. III A, we discuss the band structures of the $PuIn_3$ and $PuSn_3$ compounds, respectively. In Sec. III B, the DOS for the two compounds in concert with the band structures are discussed. In Sec. III C, we show the Fermi surface topology and the corresponding dHvA orbits, which are relevant to available experimental studies. Discussions and conclusions are summarized in Sec. IV.

II. THEORETICAL METHOD

$PuIn_3$ and $PuSn_3$ compounds crystallize into a cubic $AuCu_3$-type structure at room temperature and have an actinide-actinide distance far above the Hill limit,[12] making the $5f$-ligand hybridization the dominant mechanism for Pu $5f$-electron delocalization. The experimental lattice constants at room temperature and atmosphere pressure [4.61 Å for $PuIn_3$

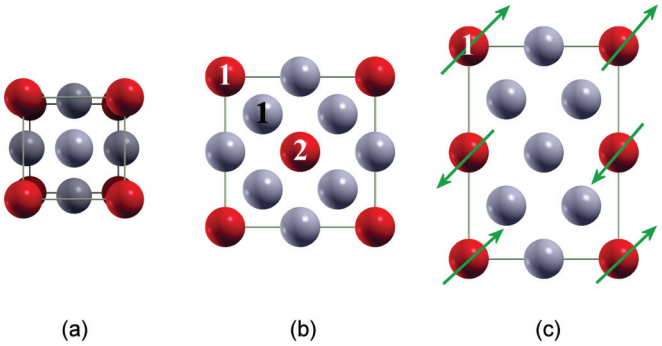

FIG. 1. (Color online) (a) PM PuM_3 (M = In,Sn) conventional unit cell. Red sphere: Pu; gray sphere: M. (b) Top view of the antiferromagnetic $PuIn_3$ conventional unit cell. (c) Side view of the AFM $PuIn_3$ conventional unit cell. The green arrows illustrate the commensurate AFM order. The tilted arrow just indicates the spontaneous symmetry breaking orientation for viewing convenience. The actual orientation for our studies can vary. The AFM unit cell is enlarged twice with respect to the PM unit cell along the top-view axis to accommodate the AFM order. The enlarged AFM unit cell coincides with two PM unit cells up to a 45° rotation with respect to the top-view axis.

(Ref. 13) and 4.63 Å for $PuSn_3$ (Ref. 14), respectively] are used in our calculation. $PuSn_3$ was reported as a paramagnet, experimentally.[15] However, $PuIn_3$ was originally assumed[11] to be paramagnetic, but more recent experiments indicate it is in an AFM state below 14 K.[10] In this work, we consider both PM and AFM cases for the $PuIn_3$ compound. The conventional unit cell of PM PuM_3 (M = In,Sn) is shown in Fig. 1(a) with the ligand atoms M situated at the face centers of the cell. The magnetic unit cell for AFM $PuIn_3$ is enlarged because it is the commensurate AFM order obeying the discrete translational invariance in the crystal. Figure 1(b) shows the top view of the magnetic unit cell accommodating the commensurate AFM order. The side view is shown in Fig. 1(c). Therefore, the lattices can be considered as a tetragonal Bravais lattice decorated with the basis of Pu and In atoms.

The first-principles calculations used here are based on the generalized gradient approximation with the Perdew-Burke-Ernzerhof 1996 (PBE96) functional.[16] It has been well known that density-functional theory under the local density approximation (LDA) underestimates the correlation effects for late actinide metals including plutonium metals, leading to a much smaller predicted atomic volume with regards to experimental values.[1] With the generalized gradient approximation (GGA), the weak exchange correlation effects are incorporated more reliably than LDA. As a consequence, the GGA prediction generally moves the atomic volume closer to experimental values since the late actinide metals are on the strongly correlated side. In this work, we are interested in plutonium-based compounds ($PuIn_3$ and $PuSn_3$). As suggested by the dominant role of majority ligand atoms in other Pu-115 compounds,[8] we confirm the experimental equilibrium configuration is reliably determined by GGA studies, with the predicted atomic volumes well under 3% error regardless of different magnetic orders. Therefore, it is legitimate for us to use the GGA approximation as a starting point to study the electronic properties of these plutonium compounds.

We use the scheme of the full-potential linear augmented plane wave basis plus local basis[17] (FP-LAPW + lo), as implemented in the WIEN2K code.[18] The LAPW sphere radii R used for Pu, In, and Sn atoms are 2.5 bohrs. The interstitial plane wave number cutoff $k_{\max}R = 8.0$ is chosen for the basis set. The semicore states (Pu $6s6p$, In $4p$) are included with the valence electrons using local orbitals. The core states are treated at the fully relativistic level with a spin-orbit coupling for all atoms. The spin-orbit couplings for semicore and valence states are incorporated by a second variational procedure[19] using the scalar relativistic eigenstates as the basis, except that the so-called $6p_{1/2}$ relativistic local orbitals[20] are used to account for the finite character of the wave function at the Pu nucleus. Dense Brillouin zone sampling is used for the calculation of the Fermi surface. We use a $31 \times 31 \times 31$ k mesh for the PM $PuIn_3$ and $PuSn_3$ calculations. A $31 \times 31 \times 22$ k mesh is used for the AFM $PuIn_3$. Experimentally, a full determination of the magnetic structure for the AFM state of $PuIn_3$ is still needed. Therefore, we assume this structure follows that of its isostructural compound, $CeIn_3$.[21,22] This choice is also supported by the Fermi surface topology of PM $PuIn_3$, as discussed later. The dHvA effect is observable in very clean metallic systems, typically in strong magnetic fields exceeding several Tesla. On sweeping the magnetic field **B**, one observes oscillations in the magnetization, which are periodic in an inverse magnetic field due to the fact that the number of occupied Landau levels changes with the magnetic field. The measurement of the dHvA effect with a varying magnetic field orientation is a powerful probe on the Fermi surface topology in metallic and intermetallic systems. The dHvA frequency F in mks units is related to the extremal Fermi surface cross-sectional area A surrounded by extremal cyclotron orbits perpendicular to the magnetic field orientation:[23]

$$F = \frac{\hbar}{2\pi e} A, \tag{1}$$

where e is the elementary charge and $\hbar$ is the reduced Planck constant. In addition, the effective mass of electrons averaged around the cyclotron orbits can be determined by the damping strength of dHvA measurements as a function of temperature. Our determination of the dHvA orbits is based on the numerical algorithm implemented by Rourke and Julian.[24]

III. RESULTS

A. Band structures

Since PM PuM_3 compounds can be generated from the cubic unit cell in space, the corresponding Brillouin zone (BZ) is cubic in reciprocal space. For simplicity, we label high-symmetry **k** points by the notation adopted by the tetragonal unit cell, as shown in Fig. 2, even though the BZ for the PM PuM_3 is cubic.

The band structure for both PM $PuIn_3$ and $PuSn_3$ demonstrates two bands across the Fermi energy. The energy dispersion along the high-symmetry points is shown in Figs. 3 and 4. We observe the Fermi energy is crossed by two bands mainly of $5f$ electron character, as shown later in the DOS studies. The f bands are far from flat due to the hybridization mainly from the $5p$ valence electron of the ligand atoms. We calculate the band structure of PM $PuIn_3$ and PM $PuSn_3$ by

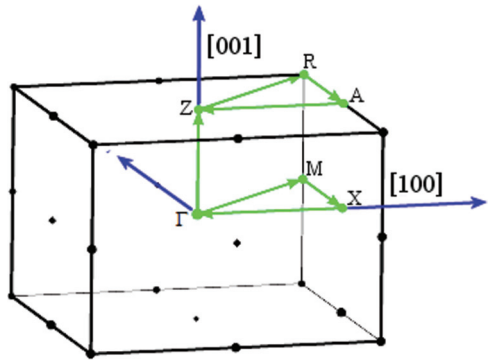

FIG. 2. (Color online) Tetragonal Brillouin zone (BZ). The symmetry points are labeled by capital letters.

the density-functional theory using the GGA approximation. We notice that the energy dispersion for PM $PuSn_3$ is very different, which indicates that the PM $PuIn_3$ and PM $PuSn_3$ have very different Fermi surface topologies, as discussed in Sec. III C.

For the AFM $PuIn_3$ with the chosen magnetic unit cell, the BZ in the reciprocal lattices becomes tetragonal. Let us first discuss the circumstances in which magnetic moment orientation $\boldsymbol{\sigma}$ for the AFM order is parallel to the [001] direction defined by the PM $PuIn_3$ crystal unit cell. There are more atoms in the unit cell and therefore many more bands are accommodated in the corresponding tetragonal BZ. We observe four bands crossing the Fermi energy E_f, as shown in Fig. 5. In this case, the bandwidth of the $5f$ bands across the Fermi surface is much narrower than the bandwidth in

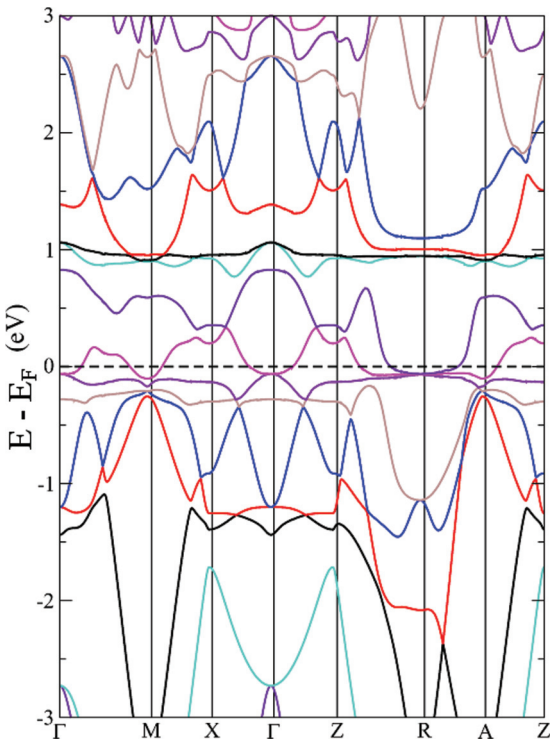

FIG. 3. (Color online) Band structure of the PM $PuIn_3$ along the high-symmetry points in BZ.

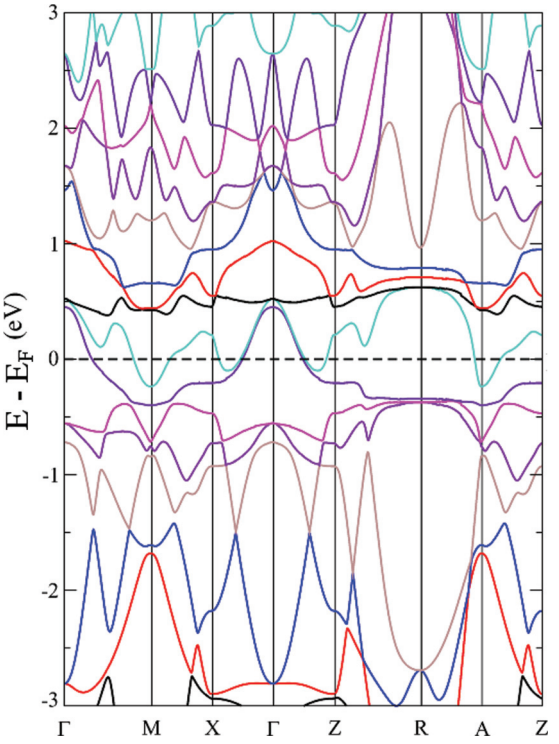

FIG. 4. (Color online) Band structure of the PM $PuSn_3$ along the high-symmetry points in cubic BZ. Two conduction bands are across the Fermi level E_F.

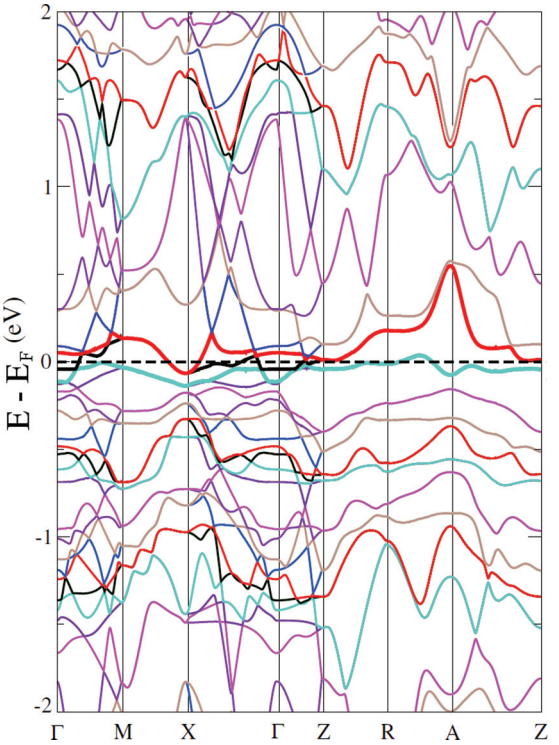

FIG. 5. (Color online) Band structure of the AFM $PuIn_3$ along the high-symmetry points in tetragonal BZ with the local spin polarization $\boldsymbol{\sigma} \parallel [001]$.

the PM case. The energy bands near the Fermi energy have dominant $5f$ electron features, as shown later in the DOS, and have a large effective band mass because of the flatness of the bands.

B. Density of states

By the smaller equilibrium volume of $PuIn_3$ in comparison with $PuSn_3$, one may argue that PM $PuIn_3$ should have more itinerant $5f$ bands in comparison with $PuSn_3$ due to the smaller distance between nearest-neighboring Pu atoms and the In atoms. In addition, the atomic $5p$ levels from the ligand atoms in $PuIn_3$ tend to be more delocalized due to a smaller attraction from the nucleon charges. However, those effects are not expected to be very remarkable in the DOS because of the closeness of the atomic properties for the In atom and Sn atom.

To understand the hybridization between the Pu $5f$ and ligand valence states, we perform the DOS calculation for these compounds. In Fig. 6, the DOS for the PM $PuIn_3$ is shown. We observe a nonzero total DOS near the Fermi level. The peak near the Fermi energy shows a hybridization of Pu $5f$ with the DOS of the $5p$ valence electrons from the In atom. This indicates that the metallic behavior is inherent from the hybridization of $5f$ localized electrons at Pu with $5p$ itinerant electrons at In. The two strong peaks away from the Fermi surface are due to the strong spin-orbit coupling for the localized f electrons, which is weakly hybridized with In $5p$ orbitals. The lower peak is mainly due to $j = 5/2$ subbands and the higher peak is mainly due to $j = 7/2$ subbands, which has been studied previously by the relativistic Stoner theory.[25] The $5f$ electron occupancy at the Pu atomic sphere is around

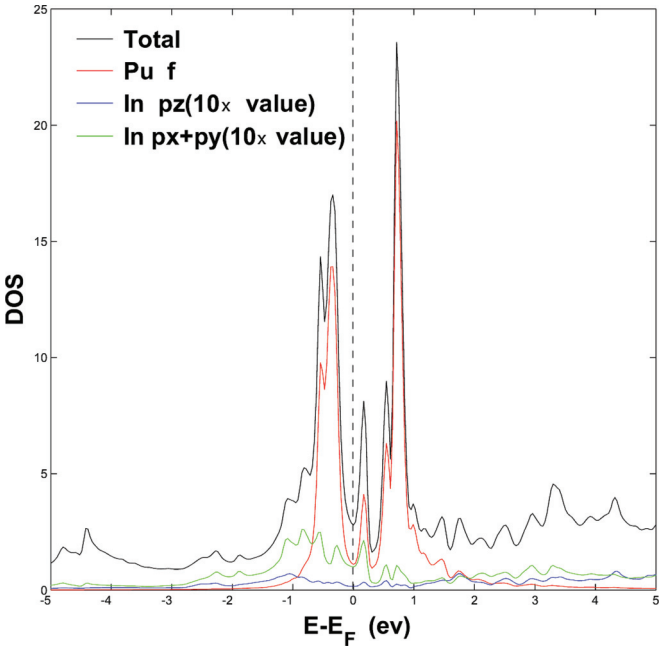

FIG. 6. (Color online) DOS per atom and total DOS in a PM $PuIn_3$ compound. Ten times of the actual density of states for the p orbitals at the In site are plotted for better contrast. The black solid line shows the total DOS in the BZ.

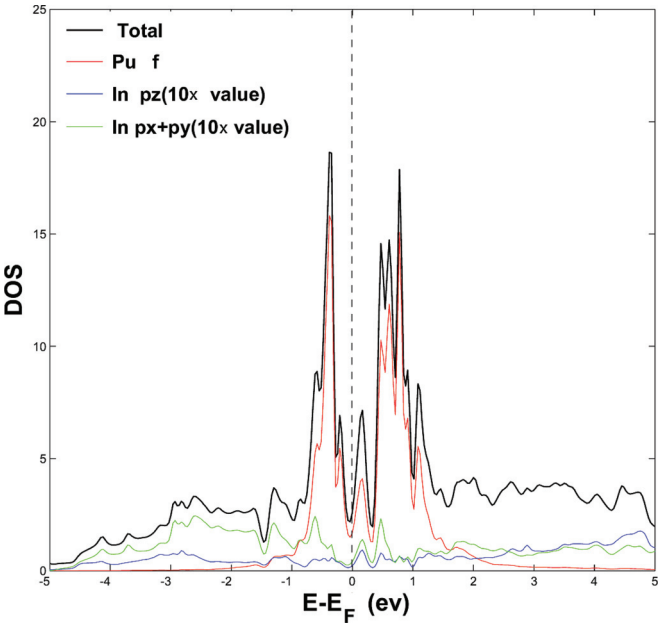

FIG. 7. (Color online) DOS per atom and total DOS in a PM $PuSn_3$ compound. Ten times of the actual DOS for the p orbitals at the Sn site are plotted for better contrast. The black solid line shows the total DOS in the BZ.

4.8. This suggests that the midpeak near the Fermi energy originates from the higher $j = 5/2$ subbands in the presence of crystal-field splitting. The three-peak features are similar also in $PuSn_3$ except the $j = 5/2$ peaks are broadened by the hybridization from the Sn p orbitals. Figure 7 presents the DOS for $PuSn_3$. We notice the $j = 5/2$ subbands are still sharply peaked but with a slightly larger $5f$ DOS at the Pu site, as shown by the solid red line, as suggested by a slightly smaller hybridization. As will be discussed later, PM $PuIn_3$ and PM $PuSn_3$ have very different Fermi surface topologies despite a similarity in the DOS.

We have also calculated the DOS for AFM $PuIn_3$, and, as shown in Figs. 1(b) and 1(c), the lattice can be divided into two sublattices. The calculated spin-projected partial DOS at different atomic sites is shown in Fig. 8. We observe that the Pu1 atom has a larger $5f$ occupancy in the up-spin channel (see the corresponding partial DOS as denoted by the blue solid line). However, the Pu2 atom takes a larger $5f$ occupancy in the down-spin channel (see the corresponding partial DOS as denoted by the blue dotted line). This indicates that the Pu1 and Pu2 atoms have magnetic moments due to $5f$ electrons, which are equal in magnitude but antiparallel in orientation. We do not observe a net magnetic moment at the In atoms according to the equal spin-projected DOS for the In1 atom, as indicated by the solid dashed curves. The AFM order has the effect of generating a gap, above the Fermi energy, between two major peaks belonging to up-spin and down-spin Pu $5f$ DOS. By our first-principles calculation, we found the orbital moment at the Pu1 atom is around $-2.1\mu_B$ (μ_B stands for Bohr magneton) but changes sign ($-2.1\mu_B$) for the Pu2 atom. The spin moment at the Pu1 and Pu2 atoms are given by $4.7\mu_B$ and $-4.7\mu_B$, respectively. We observe that the presence of magnetic order causes the mixing of $j = 5/2$ and $j = 7/2$ and

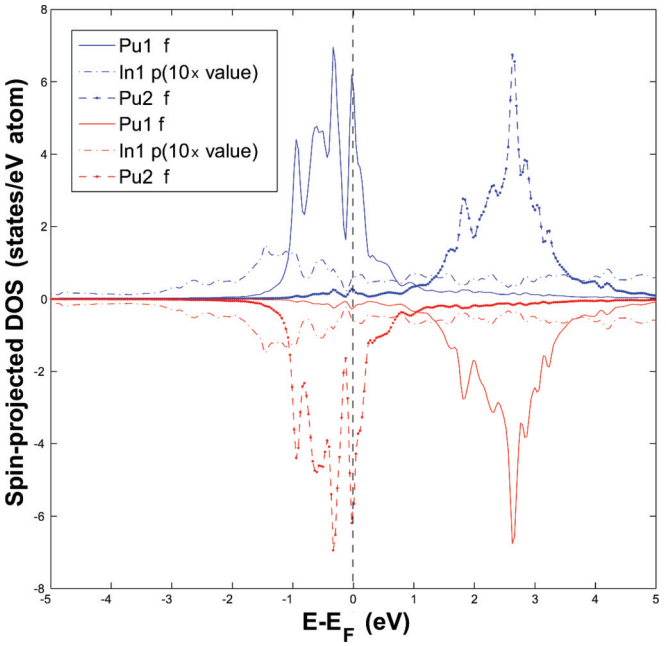

FIG. 8. (Color online) Spin-projected DOS for AFM $PuIn_3$ compound. Pu1 represents the Pu atom with a positive local magnetic moment. Pu2 represents the Pu atom with a negative local magnetic moment. It is noted that the Pu1 and Pu2 atoms are the nearest neighbors in the AFM unit cell. The In1 atom indicates the indium atom located between the Pu1 and Pu2 atoms in the unit cell [Figs. 1(b) and 1(c)]. The color blue indicates the up-spin-projected DOS along the chosen quantization $+z$ axis in the Bloch sphere. The color red indicates the down-spin-projected DOS along the $-z$ axis in the Bloch sphere. Ten times of the actual spin-projected DOS of the p orbitals at the In1 site are plotted for better contrast.

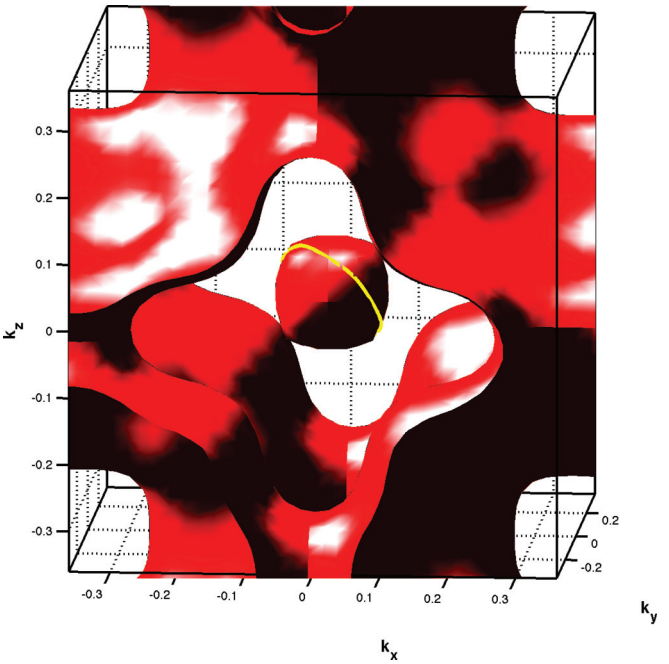

FIG. 9. (Color online) Fermi surface from band 1 in the PM $PuIn_3$ compound.

turns the local dip structure near the Fermi surface into a peak structure. In addition, two major peaks in the DOS appear away from the Fermi surface with a large energy separation between maxima.

C. Fermi surface topology and dHvA orbits

In this section, we show the Fermi surface topology and calculate the dHvA frequencies as a function of magnetic field orientation for the compounds $PuSn_3$ and $PuIn_3$. By the band structure calculation, the Fermi surface topology is determined by the isosurface calculated by the eigenstates of the Kohn-Sham equation.

1. PM $PuIn_3$ compound

The Fermi surfaces for PM $PuIn_3$ from two conduction bands are shown in Figs. 9 and 10. The ordering of bands is based on the energies in increasing order in the band dispersion (Fig. 3). There are two bands across the Fermi level. The characters of the dHvA orbits are tabulated in Tables I and II, respectively. We present the dHvA orbits of interest by the yellow orbits or the label "orbit 1" for later discussion. This is highlighted in the final two columns in Tables I and II. For band 1, when the magnetic field is chosen along the [111] direction, four types of dHvA orbits are identified in the BZ, as listed in Table I. Three of the orbits are electronlike and one is holelike. The dHvA orbit labeled as 1 originates from the Fermi surface near the center of the BZ and has a dHvA frequency $F = 0.9627$ kT. The location of orbit 1 is shown in Fig. 9

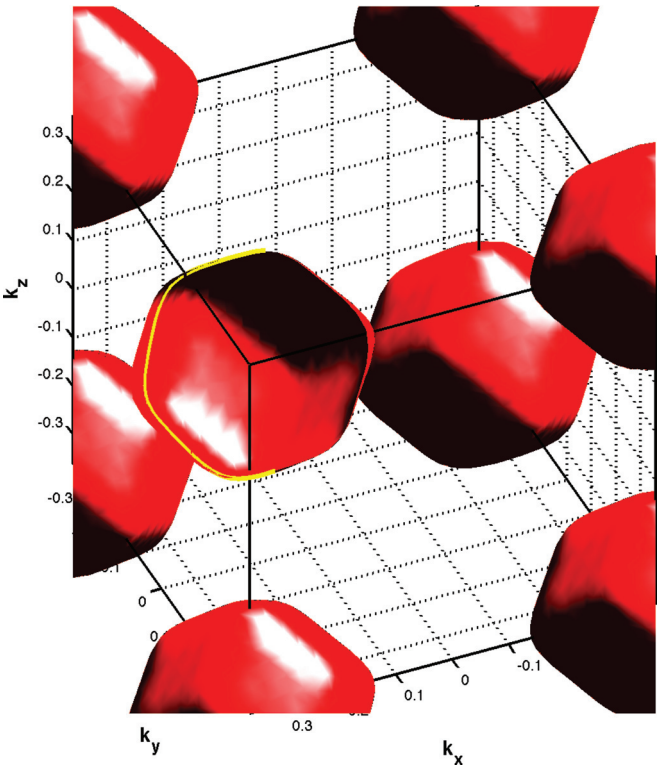

FIG. 10. (Color online) Fermi surface from band 2 in the PM $PuIn_3$ compound.

TABLE I. dHvA orbits from band 1: PM $PuIn_3$, **B** ∥ [111]. h: holelike; e: electronlike.

F (kT)	$m^*(m_e)$	Type	Number	Color	Label
16.149	6.4320	h	1		
13.209	4.9218	e	1		
10.818	6.02	e	2		
0.9627	2.4587	e	1		1

explicitly. The other orbits with much larger dHvA frequencies are not our main focus since the dHvA frequencies are far from what has been observed experimentally.[11] For band 2, only an electronlike (yellow) orbit with a dHvA frequency $F = 3.9206$ kT near the corner of the BZ is found, which is shown in Fig. 10. As far as the field angular dependence is concerned, we focus on the orbits which are connected with the same Fermi surface surrounded by the yellow orbits from band 1 and band 2 at the field orientation [111]. We observe the continuation of the orbits from the same Fermi surface spanning the whole angle range from [100] to [111] field orientation. In addition, the calculated dHvA frequencies are not close to 2 kT, as shown in Fig. 11(a). Those facts contradict the observed dHvA frequency (around 2 kT) which only survives a limited span of field angles.[11] This indicates that the assumption of the PM state in $PuIn_3$ is problematic for the interpretation of the electronic properties of the $PuIn_3$ compound. From the Fermi surface topology for PM $PuIn_3$ in Figs. 9 and 10, we notice the nesting between the small Fermi surface at the Γ point from band 1 and the four Fermi surfaces at the corners of the BZ from band 2. The nesting wave vector between the Fermi surfaces is approximately $(\pi/a,\pi/a,\pi/a)$. Therefore, the magnetic instability for a commensurate AFM order should indeed be favored. In the following, we study the commensurate AFM order in $PuIn_3$.

2. *AFM $PuIn_3$ compound*

From the band structure calculations, as shown earlier in Fig. 5, there are four bands across the Fermi level for AFM $PuIn_3$. The labeling of bands still follows the band energies (band 1, band 2, etc.). The corresponding Fermi surfaces and dHvA orbits (when the external magnetic field is orientated along the [111] direction) are illustrated in Figs. 12–15, respectively. We are interested in dHvA orbits with dHvA frequencies around 2 kT, which are labeled as orbit 1 for band 2 and band 3 in Tables IV and V. The information on the other dHvA orbits due to band 1 and band 4 are listed in Tables III and VI. We provide the Fermi surface topology for band 1 and band 4 in Figs. 12 and 15 for reference.

For band 2, the yellow orbits with a dHvA frequency of 1.3908 kT around the Fermi surface at the corner of the BZ

TABLE II. The dHvA orbit from band 2: PM $PuIn_3$, **B** ∥ [111]. h: holelike; e: electronlike.

F (kT)	$m^*(m_e)$	Type	Number of orbits	Color	Label
3.9206	3.3774	e	1	Yellow	1

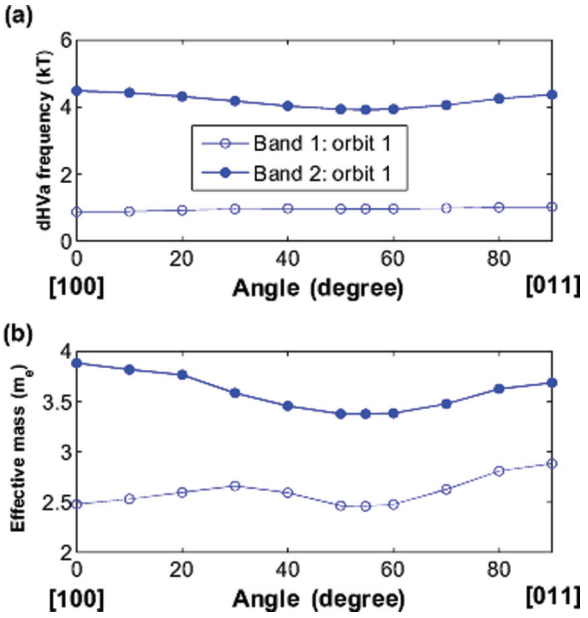

FIG. 11. (Color online) Angular dependence of dHvA frequencies and the average effective mass of the yellow orbits in the PM $PuIn_3$ compound. θ is the angle spanned from the [100] to [011] orientation at the same plane.

are illustrated in Fig. 13. When the field orientation varies, one expects dHvA orbits at different angles to be continued orbits from the same Fermi surface. Therefore, we expect the dHvA orbits inherited from the same Fermi surface to span the whole range of the angle, as shown in Fig. 16. The dHvA frequencies are lowest around the [111] orientation (angle = 54.7356°) and the value is around 1.5 kT. The effective band mass is around $5m_e$, where m_e is the free electron mass. For band 3, in Fig. 14, the dHvA frequencies around 2.3 kT spanned through a limited range of angles around [111], as can be understood by the shape of the corresponding Fermi surface. The dHvA frequencies have local maxima around the [111] orientation instead. The effective mass is above $10m_e$. Even though we have a good agreement with the experiment[11] on

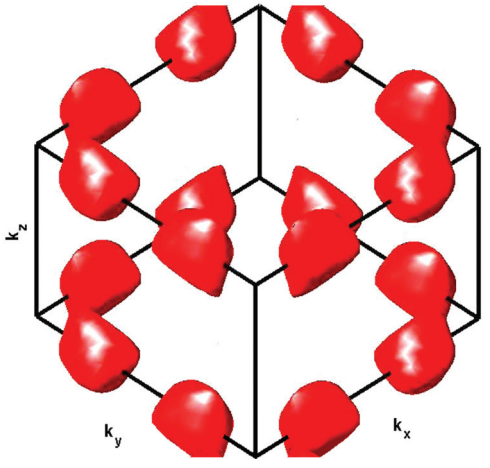

FIG. 12. (Color online) Fermi surface from band 1 in AFM $PuIn_3$ compounds with the local spin polarization $\boldsymbol{\sigma}$ ∥ [001].

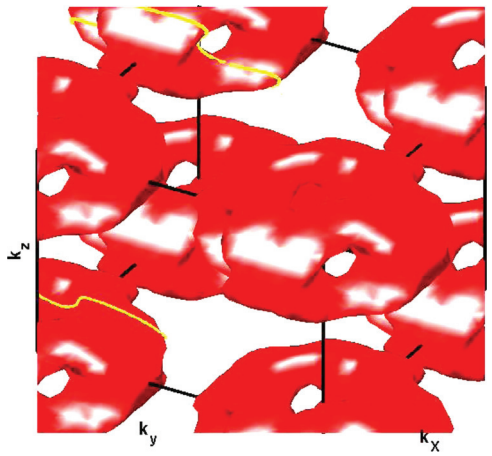

FIG. 13. (Color online) Fermi surface from band 2 in AFM $PuIn_3$ compounds with the local spin polarization $\boldsymbol{\sigma}$ ∥ [001].

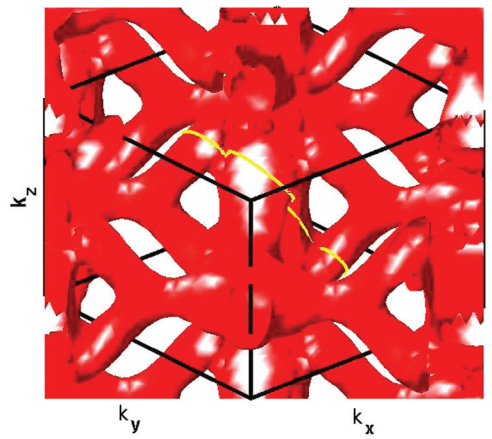

FIG. 14. (Color online) Fermi surface from band 3 in AFM $PuIn_3$ compounds with the local spin polarization $\boldsymbol{\sigma}$ ∥ [001].

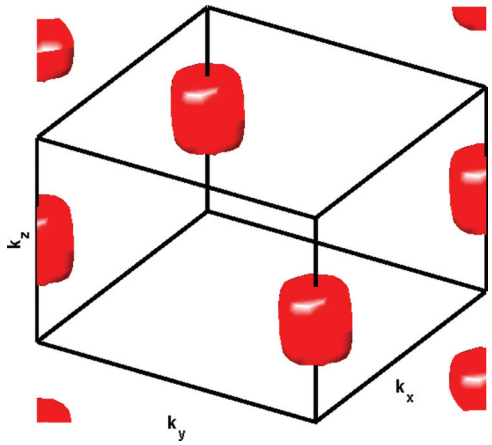

FIG. 15. (Color online) Fermi surface from band 4 in AFM $PuIn_3$ compounds with the local spin polarization $\boldsymbol{\sigma}$ ∥ [001].

TABLE III. The dHvA orbit from band 1: AFM $PuIn_3$, **B** ∥ [111], $\boldsymbol{\sigma}$ ∥ [001]. h: holelike; e: electronlike.

F (kT)	$m^*(m_e)$	Type	Number of orbits
0.4424	2.1654	h	2
0.4412	2.3620	h	2

TABLE IV. dHvA orbits from band 2: AFM $PuIn_3$, **B** ∥ [111], $\boldsymbol{\sigma}$ ∥ [001]. h: holelike; e: electronlike.

F (kT)	$m^*(m_e)$	Type	Number of orbits	Color	Label
1.3908	6.2948	h	2	Yellow	1
1.006	3.7899	h	2		
0.5189	2.6069	h	2		
0.3335	2.2621	h	4		

TABLE V. dHvA orbits from band 3: AFM $PuIn_3$, **B** ∥ [111], $\boldsymbol{\sigma}$ ∥ [001]. h: holelike; e: electronlike.

F (kT)	$m^*(m_e)$	Type	Number of orbits	Color	Label
2.3615	13.4852	e	1	Yellow	1
0.7796	1.8097	e	2		
0.6833	3.0840	e	2		
0.577	11.017	e	2		
0.2279	2.2562	e	4		
0.0386	0.8525	e	2		

TABLE VI. The dHvA orbit from band 4: AFM $PuIn_3$, **B** ∥ [111], $\boldsymbol{\sigma}$ ∥ [001]. h: holelike; e: electronlike.

F (kT)	$m^*(m_e)$	Type	Number of orbits
0.5277	1.0592	e	1

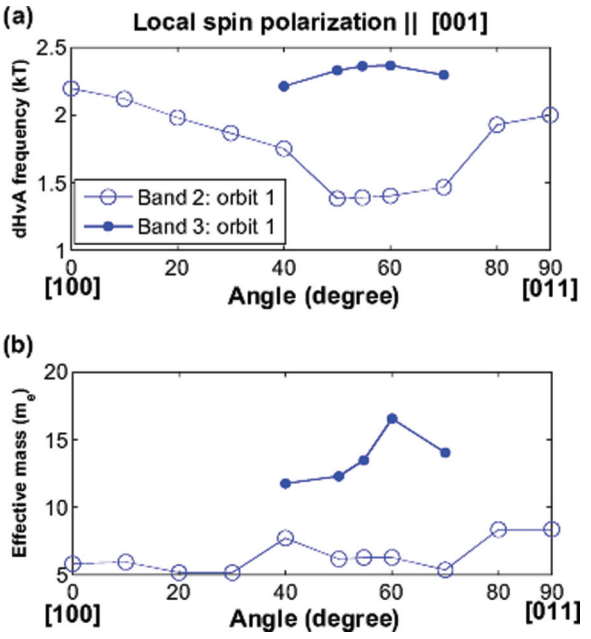

FIG. 16. (Color online) Angular dependence of dHvA frequencies and the effective mass of chosen yellow orbits for the AFM $PuIn_3$ compound.

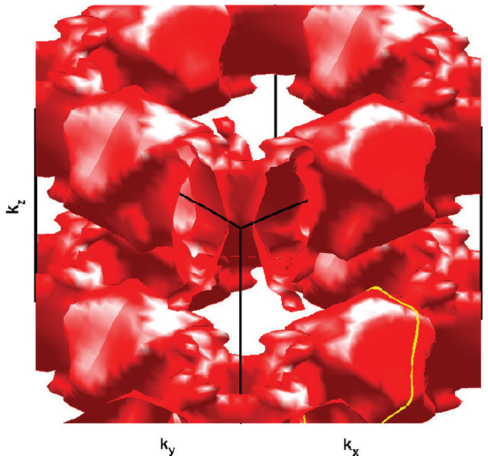

FIG. 17. (Color online) Fermi surface from band 1 in AFM $PuIn_3$ compounds with the spin polarization $\boldsymbol{\sigma} \parallel [101]$.

the dHvA frequencies with a limited angle span, the predicted dHvA frequencies have a local maxima instead of a minimum as observed experimentally. There is uncertainty in assuming the magnetization orientation of the AFM order along the [001] orientation. We expect the orientation of the magnetic order will lead to qualitative effects on the Fermi surface topology because of the strong spin-orbit coupling effects in $PuIn_3$ compounds.

Therefore, we have also considered an easy axis of magnetization along the [101] direction. In this case, we predict three $5f$ bands across the Fermi level. We show the Fermi surface topology corresponding to three bands across the Fermi level in Figs. 17–19. The details of the dHvA orbits along [111] orientation are shown in Tables VII–IX. We identify an orbit with dHvA frequency $F = 2.125$ kT, which is marked by a yellow trace in the Fermi surface around the Γ point from band 2 in Fig. 18. By the calculated angular dependence of the dHvA orbits for band 2 in Fig. 20(a), we identify that the dHvA orbits are limited to a certain angle range around

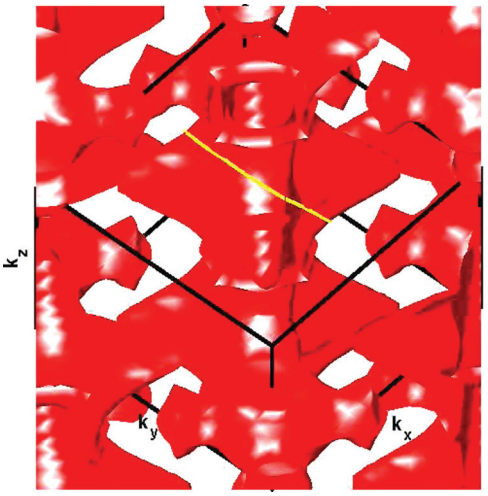

FIG. 18. (Color online) Fermi surface from band 2 in AFM $PuIn_3$ compounds with the spin polarization $\boldsymbol{\sigma} \parallel [101]$.

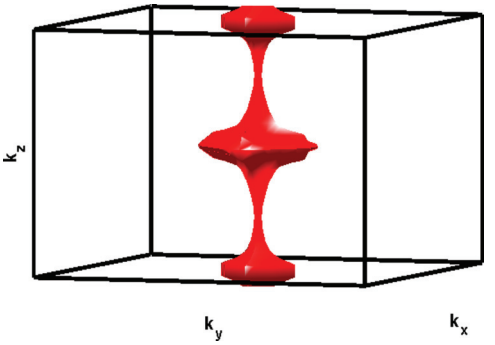

FIG. 19. (Color online) Fermi surface from band 3 in AFM $PuIn_3$ compounds with the spin polarization $\boldsymbol{\sigma} \parallel [101]$.

the [111] orientation. In addition, the effective mass have a local minima around the [111] orientation, as suggested by experiment.[11] However, the effective mass is only about $2m_e$. For the dual nature of the $5f$ electrons, the temporal quantum fluctuations can dramatically renormalize the effective band mass. We do not expect that the density-functional theory as presented in this paper can capture this effect.

As far as the calculated DOS is concerned in comparison to experimental photoemission measurements,[26] we find a good agreement at the Fermi level with a noticeable DOS (see Fig. 21) as opposed to the small DOS in PM $PuIn_3$ (see Fig. 6). In addition, we also see a main feature below the Fermi surface around -5 eV due to delocalized bands. However, by our GGA calculation, we observe a much sharper spectral feature between $E - E_F = -2$ eV and the Fermi level. This is due to the failure of GGA to treat the localized strong correlation in Pu f orbitals. The strong correlation is expected to broaden the spectral features and renormalize the DOS obtained by GGA closer to the experimental observation. This effect should be captured by other more advanced approaches to treat the strong correlation, such as dynamical mean-field theory (DMFT).[27]

3. PM $PuSn_3$ compound

So far, dHvA effects still need to be successfully observed in $PuSn_3$ compounds. By our calculation, we find multiple dHvA orbits in a narrow range of frequencies at the field orientation [111]. This may cause complications in observing clean signals. However, we do find a simple Fermi surface topology at the field orientation [001], which can be easier to observe, and thus is the case we focus on in this section. With the $PuSn_3$ band structure in Fig. 4, we observe two energy bands crossing the Fermi energy E_F, which only have a similar dispersion as PM $PuIn_3$ near the point $\Gamma = (0,0,0)$ in

TABLE VII. The dHvA orbit from band 1: AFM $PuIn_3$, $\mathbf{B} \parallel [111], \boldsymbol{\sigma} \parallel [101]$. h: holelike; e: electronlike.

F (kT)	$m^*(m_e)$	Type	Number of orbits	Color	Label
3.2569	5.8858	h	1		
1.7165	1.9391	h	1	Yellow	1
0.9876	3.4407	h	2		
0.9697	2.8944	h	2		
0.8421	3.5473	h	2		

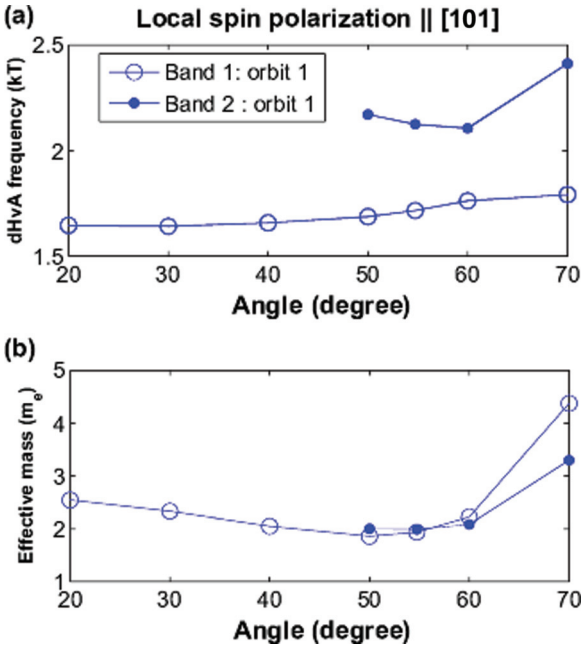

FIG. 20. (Color online) Angular dependence of dHvA frequencies and effective mass of the chosen yellow orbits for the AFM $PuIn_3$ compound. Notice that the predicted dHvA frequencies for band 2 only exist between 50° and 70°, as shown by the solid circles.

the BZ. The cutting points at the Fermi energy in Fig. 4 are the projection of the three-dimensional Fermi surface plot along the line between the symmetry points in the BZ. We show the Fermi surfaces for those two bands in Figs. 22 and 23, respectively. Our calculation shows one holelike (yellow) orbit (with $F = 3.273$ kT) near the Γ point in the BZ, which agrees with the band dispersion at band 1 near the Γ point. For band 2, the four dHvA orbits are identified and all of them are holelike at the field orientation [001] (see Table VIII), denoted by the colored solid curves in Fig. 23. The maximum dHvA frequency is given by the white cyclotron orbit with $F = 1.312$ kT near the M point in the BZ. By observing the Fermi points and the band dispersion nearby for band 2 in Fig. 4, one can see agreement with the Fermi surface. In addition, from the Fermi surface topology, one can see there is no clear evidence for a dominant Fermi surface nesting. This might explain the absence of magnetism in $PuSn_3$.[15]

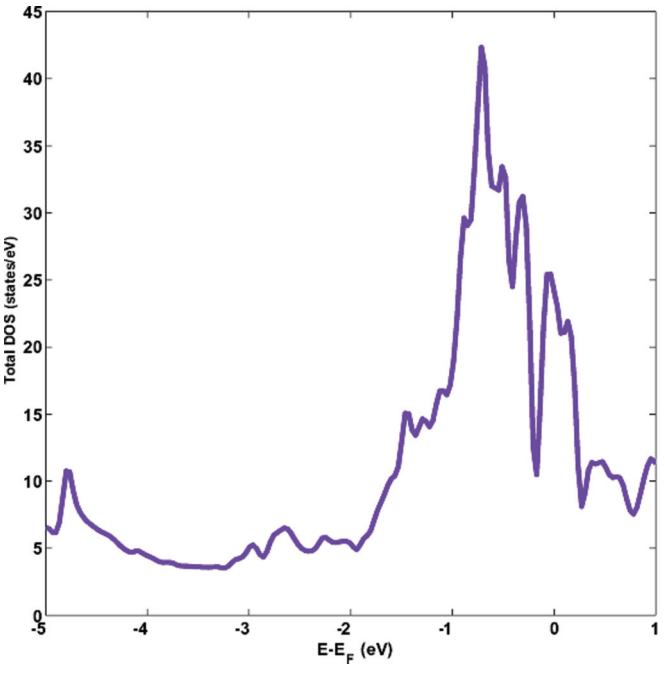

FIG. 21. (Color online) Total DOS in AFM $PuIn_3$ compounds with the spin polarization $\sigma \parallel [101]$.

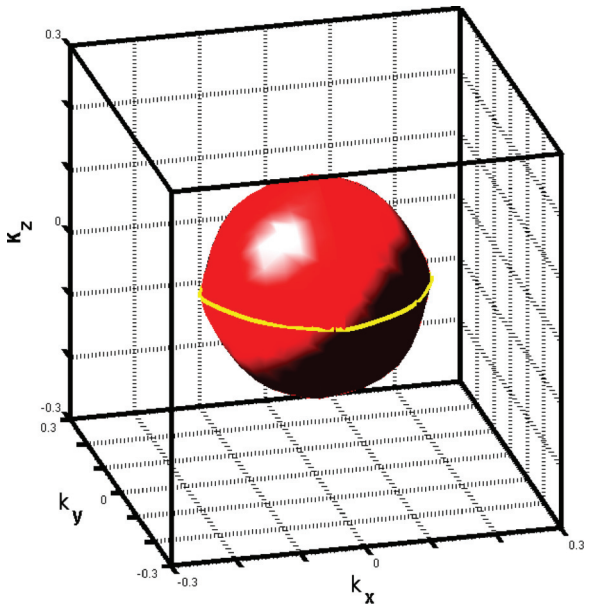

FIG. 22. (Color online) Fermi surface from band 1 in the PM $PuSn_3$ compound.

In Fig. 24, we show the field-angle dependence of dHvA frequencies for the yellow dHvA orbit in band 1 and the white dHvA orbit in band 2. The magnetic field varies from the crystal orientation [100] to [001] in the $PuSn_3$ compound. We observe that the dHvA frequencies are symmetrical with respect to the orientation at an angle 45°. The dHvA frequency for band 1 is insensitive to the orientation because of the corresponding spherical Fermi surface near the Γ point and is well separated in frequencies from the orbits due to band 2. However, the Fermi surface circled by the white orbit in band 2 is not spherical (shown in Fig. 23); therefore, a strong field-angle dependence due to the Fermi surface is obtained. The nature of dHvA orbits are given in Tables X and XI respectively for band 1 and band 2.

TABLE VIII. dHvA orbits from band 2: AFM $PuIn_3$, $\mathbf{B} \parallel [111], \sigma \parallel [101]$. h: holelike; e: electronlike.

F (kT)	$m^*(m_e)$	Type	Number of orbits	Color	Label
3.7022	6.2443	e	1		
2.1250	1.9877	e	1	Yellow	1
1.2687	2.8742	e	2		
1.1595	1.5520	e	1		
1.0834	1.7674	e	2		

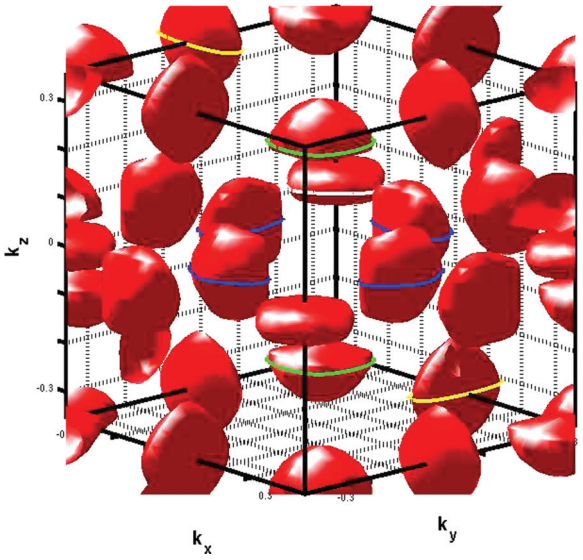

FIG. 23. (Color online) Fermi surface from band 2 in the PM $PuSn_3$ compound.

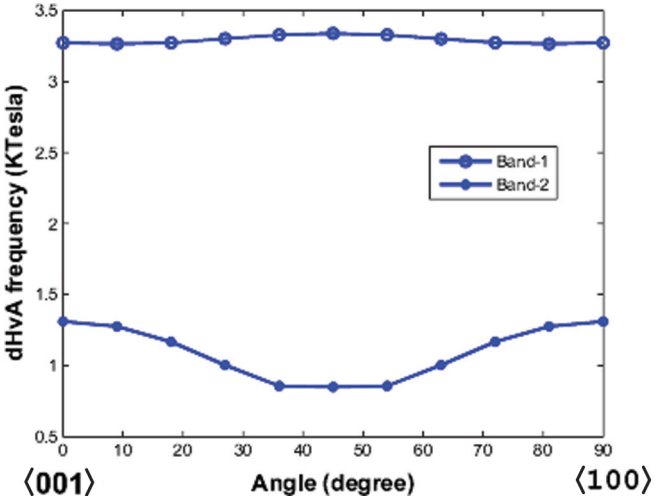

FIG. 24. (Color online) Angular dependence of dHvA frequencies in the PM $PuSn_3$ compound. The dHvA orbit of band 1 is inherent from the same Fermi surfaces circled by the yellow orbit in Fig. 17. The dHvA orbit of band 2 at different angles is inherent from the same Fermi surfaces circled by the green orbits in Fig. 18.

TABLE IX. dHvA orbits from band 3: AFM $PuIn_3$, **B** ∥ [111], σ ∥ [101]. h: holelike; e: electronlike.

F (kT)	$m^*(m_e)$	Type	Number
0.3359	2.3248	e	1
0.3358	2.4819	e	1
0.3056	2.1990	e	1
0.1935	1.7949	e	1

TABLE X. The dHvA orbit from band 1: PM $PuSn_3$, **B** ∥ [001]. h: holelike; e: electronlike.

F (kT)	$m^*(m_e)$	Type	Number of orbits	Color
3.273	1.5976	h	1	Yellow

TABLE XI. dHvA orbits from band 2: PM $PuSn_3$, **B** ∥ [001]. h: holelike; e: electronlike.

F (kT)	$m^*(m_e)$	Type	Number of orbits	Color
0.5550	0.4749	h	2	Yellow
0.6873	0.7955	h	4	Blue
1.230	1.6842	h	2	Green
1.312	0.8721	h	1	White

IV. CONCLUSIONS AND DISCUSSIONS

We study the electronic properties for the compounds $PuSn_3$ and $PuIn_3$ within the density-functional theory under the GGA approximation. Our calculations for AFM $PuIn_3$, with magnetization along the [001] direction, show that the Fermi surfaces with a heavy effective band mass produce dHvA frequencies near 2 kT, in quantitative agreement with experiments, but the field-angle dependence of dHvA frequencies around the [111] orientation (≈54.74°) cannot be reconciled with experiment. However, when the magnetization aligns along the [101] direction, we can identify different orbits showing good agreement with dHvA measurements. We point out the predicted effective band mass values can be further renormalized due to temporal quantum fluctuations which cannot be captured properly with the density-functional theory. Experimental investigations of the effective band mass of the dHvA orbits and the magnetic order are crucial to those issues.

In addition, we predict the band structure and dHvA frequencies for $PuSn_3$, which is known to be paramagnetic, for guiding the search for dHvA effects in $PuSn_3$ intermetallic compounds. Experimental observation of these frequencies in the compound will help the search for quantum oscillations in the δ phase of Pu. As a known fact, the GGA underestimates the electronic correlations in complex materials. The evaluation of these effects on electron mass and the Fermi surface in the compounds studied here requires a more rigorous but sophisticated quantum many-body approach and goes beyond the scope of the present study.

Finally, we comment on the factors that are pertinent to the observation of predicted dHvA orbits. When the dHvA frequency is too low, the temperature required to observe the well-defined quantum oscillations has to be much lower than the energy scale set by the cyclotron frequency. It poses a challenge to the experimental observation. The other constraint is set by the sample size. When the dHvA frequency is too low, the corresponding cyclotron radius can be much larger than the sample size, making its observation difficult. In addition, for high frequency orbits, the sample quality is extremely important. Any scattering due to impurities can damp out the dHvA oscillations within the cycle of quantum oscillation. We believe that the capability and design of the experiments limit what can be observed in reality.

ACKNOWLEDGMENTS

We thank Eric D. Bauer, Ross D. McDonald, Matthias J. Graf, and P. M. C. Rourke for helpful discussions. This work was supported by U.S. DOE at LANL under Contract No. DE-AC52-06NA25396 and LANL LDRD-DR Program (C.-C.W. and J.-X.Z.).

[1]K. T. Moore and G. van der Laan, Rev. Mod. Phys. **81**, 235 (2009).
[2]A. M. Boring and J. L. Smith, Los Alamos Sci. **26**, 91 (2000).
[3]Y. Wang and Y. F. Sun, J. Phys.: Condens. Matter **12**, L311 (2000).
[4]G. Robert, A. Pasturel, and B. Siberchicot, Phys. Rev. B **68**, 075109 (2003).
[5]J. L. Sarrao, L. A. Morales, J. D. Thompson, B. L. Scott, G. R. Stewart, F. Wastin, J. Rebizant, P. Boulet, E. Colineau, and G. H. Lander, Nature (London) **420**, 297 (2002).
[6]F. Wastin, P. Boulet, J. Rebizant, E. Colineau, and G. H. Lander, J. Phys.: Condens. Matter **15**, S2279 (2003).
[7]E. D. Bauer, M. M. Altarawneh, P. H. Tobash, K. Gofryk, O. E. Ayala-Valenzuela, J. N. Mitchell, R. D. McDonald, C. H. Mielke, F. Ronning, J. C. Griveau, E. Colineau, R. Eloirdi, R. Caciuffo, B. L. Scott, O. Janka, S. M. Kauzlarich, and J. D. Thompson, J. Phys.: Condens. Matter **24**, 052206 (2012).
[8]J.-X. Zhu, P. H. Tobash, E. D. Bauer, F. Ronning, B. L. Scott, K. Haule, G. Kotliar, R. C. Albers, and J. M. Wills, Europhys. Lett. **97**, 57001 (2012).
[9]I. Opahle and P. M. Oppeneer, Phys. Rev. Lett. **90**, 157001 (2003).
[10]H. Yasuoka *et al*. (unpublished); C. H. Booth, Y. Jiang, D. L. Wang, J. N. Mitchell, P. H. Tobash, E. D. Bauer, M. A. Wall, P. G. Allen, D. Sokaras, D. Nordlund, T.-C. Weng, M. A. Torrez, and J. L. Sarrao, Proc. Natl. Acad. Sci. U.S.A. **26**, 10205 (2012).
[11]Y. Haga, D. Aoki, H. Yamagami, T. D. Matsuda, K. Nakajima, Y. Arai, E. Yamamoto, A. Nakamura, Y. Homma, Y. Shiokawa, and Y. Ōnuki, J. Phys. Soc. Jpn. **74**, 2889 (2005).
[12]H. H. Hill, in *Plutonium 1970 and Other Actinides*, edited by W. N. Miner (AIME, New York, 1970), p. 2.
[13]F. H. Ellinger, C. C. Land, and K. A. Johnson, Trans. Metall. Soc. AIME **233**, 1252 (1965).
[14]S. M. Baizaee and A. Pourghazi, Physica B **387**, 287 (2007).
[15]V. Sechovsky' and L. Havela, in *The Handbook of Ferromagnetic Materials*, edited by E. P. Wohlfarth and K. H. J. Buschow (North-Holland, Amsterdam, 1988), Vol. 4.
[16]J. P. Perdew, K. Burke, and M. Ernzerhof, Phys. Rev. Lett. **77**, 3865 (1996).
[17]E. Sjostedt, L. Nordstrom, and D. J. Singh, Solid State Commun. **114**, 15 (2000).
[18]P. Blaha, K. Schwarz, G. Madsen, D. Kvasnicka, and J. Luitz, *WIEN2K, An Augmented Plane Wave + Local Orbitals Program for Calculating Crystal Properties* (Techn. Universität Wien, Austria, 2001).
[19]D. D. Koelling and B. N. Harmon, J. Phys. C **10**, 3107 (1977).
[20]J. Kunes, P. Novak, R. Schmid, P. Blaha, and K. Schwarz, Phys. Rev. B **64**, 153102 (2001).
[21]J. M. Lawrence and S. M. Shapiro, Phys. Rev. B **22**, 4379 (1980).
[22]N. D. Mathur, F. M. Grosche, S. R. Julian, I. R. Walker, D. M. Freye, R. K. W. Haselwimmer, and G. G. Lonzarich, Nature (London) **394**, 39 (1998).
[23]D. Shoenberg, *Magnetic Oscillations in Metals* (Cambridge University Press, Cambridge, U.K., 1984).
[24]P. M. C. Rourke and S. R. Julian, Comput. Phys. Commun. **183**, 324 (2012).
[25]O. Eriksson, M. S. S. Brooks, and B. Johansson, Phys. Rev. B **39**, 13115 (1989).
[26]J. J. Joyce, J. M. Wills, T. Durakiewicz, M. T. Butterfield, E. Guziewicz, D. P. Moore, J. L. Sarrao, L. A. Morales, A. J. Arko, O. Eriksson, A. Delin, and K. S. Graham, Physica B **378–380**, 920 (2006).
[27]G. Kotliar, S. Y. Savrasov, K. Haule, V. S. Oudovenko, O. Parcollet, and C. A. Marianetti, Rev. Mod. Phys. **78**, 865 (2006).